NANO · MICRO small
www.small-journal.com

Static and Dynamic Self-Assembly of Pearl-Like-Chains of Magnetic Colloids Confined at Fluid Interfaces

Fernando Martínez-Pedrero, Andrés González-Banciella, Alba Camino, Ana Mateos-Maroto, Francisco Ortega, Ramón G. Rubio, Ignacio Pagonabarraga, and Carles Calero**

Magnetic colloids adsorbed at a fluid interface are unique model systems to understand self-assembly in confined environments, both in equilibrium and out of equilibrium, with important potential applications. In this work the pearl-chain-like self-assembled structures of superparamagnetic colloids confined to a fluid–fluid interface under static and time-dependent actuations are investigated. On the one hand, it is found that the structures generated by static fields transform as the tilt angle of the field with the interface is increased, from 2D crystals to separated pearl-chains in a process that occurs through a controllable and reversible zip-like thermally activated mechanism. On the other hand, the actuation with precessing fields about the axis perpendicular to the interface induces dynamic self-assembled structures with no counterpart in non-confined systems, generated by the interplay of averaged magnetic interactions, interfacial forces, and hydrodynamics. Finally, how these dynamic structures can be used as remotely activated roller conveyors, able to transport passive colloidal cargos at fluid interfaces and generate parallel viscous flows is shown. The latter can be used in the mixture of adsorbed molecules and the acceleration of surface-chemical reactions, overcoming diffusion limitations.

1. Introduction

Superparamagnetic colloids have been extensively used to generate tunable self-assembled structures. Due to the precise control in their fabrication–size, shape, magnetic properties– and the capacity to externally modulate their interaction, magnetic particles are suitable model systems to investigate self-assembly processes both in equilibrium an out of equilibrium.[1–7] Understanding the aggregation of magnetic particles is also essential for their use in the fabrication of metamaterials,[8] as magnetic separation agents in, e.g., protein purification protocols,[9] as contrast agents in magnetic resonance imaging,[10] or as cell manipulation operators[11] among others.

Floating magnetic particles have also been extensively used in the bottom-up fabrication of different dynamic self-assemblies, which develop order at the same time as dissipate energy. The strong confinement of a system of particles can dramatically influence both the nature of their interactions and the long-range order possible, permitting the existence of new structures and phases both in equilibrium[12,13] and out of equilibrium.[12,14] Besides, the quasi 2D nature of these systems facilitates the experimental analysis of the structure and dynamics. In this regard, magnetic colloids adsorbed at liquid–liquid interphases have been proven to be suitable model systems to investigate the formation of static and dynamic arrangements of particles, and promising candidates to engineer novel functional planar structures unfeasible in bulk dipolar systems.[15,16,17] Grzybowski et al. studied disparate dynamic structures formed by rotating millimeter-sized magnetic disks, in processes ruled by the equilibrium between

Dr. F. Martínez-Pedrero, A. González-Banciella, A. Camino, Dr. A. Mateos-Maroto, Prof. F. Ortega, Prof. R. G. Rubio
Departamento de Química-Física
Universidad Complutense de Madrid
Avda. Complutense s/n, Madrid 1, Madrid 28040, Spain
E-mail: fernandm@ucm.es

Prof. F. Ortega, Prof. R. G. Rubio
Inst. Pluridisciplinar
Universidad Complutense de Madrid
Paseo Juan 23,1, Madrid 2, Madrid 28040, Spain

The ORCID identification number(s) for the author(s) of this article can be found under https://doi.org/10.1002/smll.202101188.

DOI: 10.1002/smll.202101188

Prof. I. Pagonabarraga, Dr. C. Calero
Departament de Física de la Matèria Condensada
Universitat de Barcelona
Barcelona 08028, Spain
E-mail: carles.calero@ub.edu

Prof. I. Pagonabarraga
Universitat de Barcelona Institute of Complex Systems (UBICS)
Universitat de Barcelona
Barcelona 08028, Spain

Prof. I. Pagonabarraga
CECAM
Ecole Polytechnique Federale de Lausanne
Batochime, Avenue Forel 2, Lausanne 1015, Switzerland

Dr. C. Calero
Institut de Nanociència i Nanotecnologia
IN2UB
Universitat de Barcelona
Barcelona 08028, Spain

magnetic attraction and hydrodynamic repulsion.[18] In a slightly different system, spinning ferromagnetic microdiscs with sinusoidal edge-height profiles exhibited both attractive and repulsive capillary interactions, which can be overcome by the torque generated via a fast-rotating field. Here, the change of the rotational velocity of the field induced the assembling and disassembling of the monolayer in different configurations, ultimately determined by the directionality of the capillary interactions.[19] Snezhko et al. reported on dynamic snake-like and aster-like structures, formed via the application of an out of plane oscillatory field, due to the coupling between the surface waves generated at the fluid interface and the magnetic response of the particles.[16] They also explored pulsating clusters, single-particle-thick linear aggregates and/or dynamic monolayers of equally sized spinners generated when energized by an in-plane alternating field, at different amplitude and frequency of the applied field.[20]

When the magnetic micron-sized particles adsorb to a fluid–fluid surface, the trapping surface energy is typically orders of magnitude higher than both thermal and magnetostatic energy.[12] Hence, the translational motion of the particles occurs on the fluid interface while rotations are restricted to occur around the axis perpendicular to the plane of the interface, even when the particles are torqued by an external field.[21] As a result of the strong confinement, magnetic particles self-assemble in a set of unique arrangements, determined by the contact angle at the particle's surface, the actuation of the applied field and the anisotropic character of the magnetic interactions.[17,22] Under a constant field normal to the interface, the confined particles interact via a soft centrosymmetric dipole–dipole repulsion, which induces spatial ordering in relatively dense monolayers of monodisperse particles. In crowded conditions, such systems were shown to gradually pass through the three phases predicted by the Kosterlitz-Thouless-Halperin-Nelson-Young (KTHNY) theory -liquid, hexatic and hexagonal solid- as the ratio between the pair interaction and the kinetic energy of each bead increases, as a result of the progressive increase of the external field.[15] The tilting of the applied field with respect to the confining surface can reversibly transform the hexagonal order of the floating crystals into metastable structures with other planar crystal symmetries, such as oblique, centered-rectangular, rectangular and square lattices.[23] It can also promote the unzipping of chains laterally aggregated, the partial fragmentation of the chains or the gradual separation of the monomers and the abrupt colloidal explosion. The different dismantling mechanisms are mainly governed by the tilt angle, but also heavily influenced by the thermal energy, the contact angle of the particles and the local magnetization.[22]

To further investigate how 2D confinement determines static and dynamic self-assembly when colloids exhibit anisotropic interactions, we have performed a series of experiments in which magnetic microparticles adsorbed to a fluid interface were energized by applying constant and precessing fields, while continuously monitored with bright-field light microscopy. At this spatial scale, unlike the conditions prevailing when using larger particles,[16,21] the detachment energy dominates over the magnetic, electrostatic, gravitational or inertial counterparts, and the confining boundary imposes a new plane of symmetry. Therefore, we will focus on the crucial role to be played by the orientation of the externally controlled field and analyze the effect of mutual time-averaged dipolar interactions has on the floating colloids. Due to the superparamagnetic character of the particles, magnetic dipole–dipole interactions only emerge in the presence of an external field, so we will also pay special attention to the time evolution of the transient structures that arise after applying the field, before reaching steady states. The findings could be useful in the design of new colloidal architectures, with new functionalities, while helping to explain the structures and transitions that are achieved when the particles are suspended in a viscous medium, with freedom of movement in three dimensions.

2. Results and Discussion

2.1. Static Self-Assembly of Floating Pearl Chains

2.1.1. Experimental Findings

Before the application of any external magnetic field, the micron-sized particles adsorbed at the fluid interface diffuse along the confining plane (see the Experimental Section), bearing a viscous drag unexpectedly larger than that felt in the bulk.[24] In the conditions of our experiments, the adsorbed particles are mostly immersed in the aqueous phase (see the SEM images of the magnetic particles obtained with the Gel Trapping Technique (GET) in ref. [22]). Hence, they do not display order due to long-ranged dipole–dipole electrostatic repulsions,[25] neither aggregate due to capillary interactions, even at high surface coverages.[26] The application of a constant field parallel to the interface induces the magnetization of paramagnetic particles, and promotes the formation of linear aggregates oriented along the field direction.[2,27] As the particle number density and field strength increase, a range of structures are formed, from a disordered liquid phase to one-particle-thick linear chains and wider fibrous structures, made up of bundles of zippered chains in which particles in adjacent chains are disposed out of registry by a radius distance.[1,2] Due to the superparamagnetic character of the components, all the described structures are stable only under the presence of the external field, while immediately disintegrate due to thermal fluctuations once the applied field is switched off.

The magnetic energies, in the order of tens of k_BT, are much smaller than interfacial energies, in the order of millions of k_BT. Consequently, the paramagnetic particles are forced to remain confined on a flat surface, and the reorientation of the field out of the interface does not promote the out-of-plane rotation of the spheres, but the dipolar repulsion between the particles and the appearance of different disaggregation mechanisms. **Figure 1**a shows the structures observed when bundles of superparamagnetic microparticles, previously formed under the influence of a field H_x applied in the plane of the interface, are exposed to static magnetic fields with different values of the component of the field perpendicular to the interface H_z. In zone I of Figure 1a, the particles maintain the formation of chains and bundles oriented along the horizontal component of the applied field. The gradual increase of the perpendicular

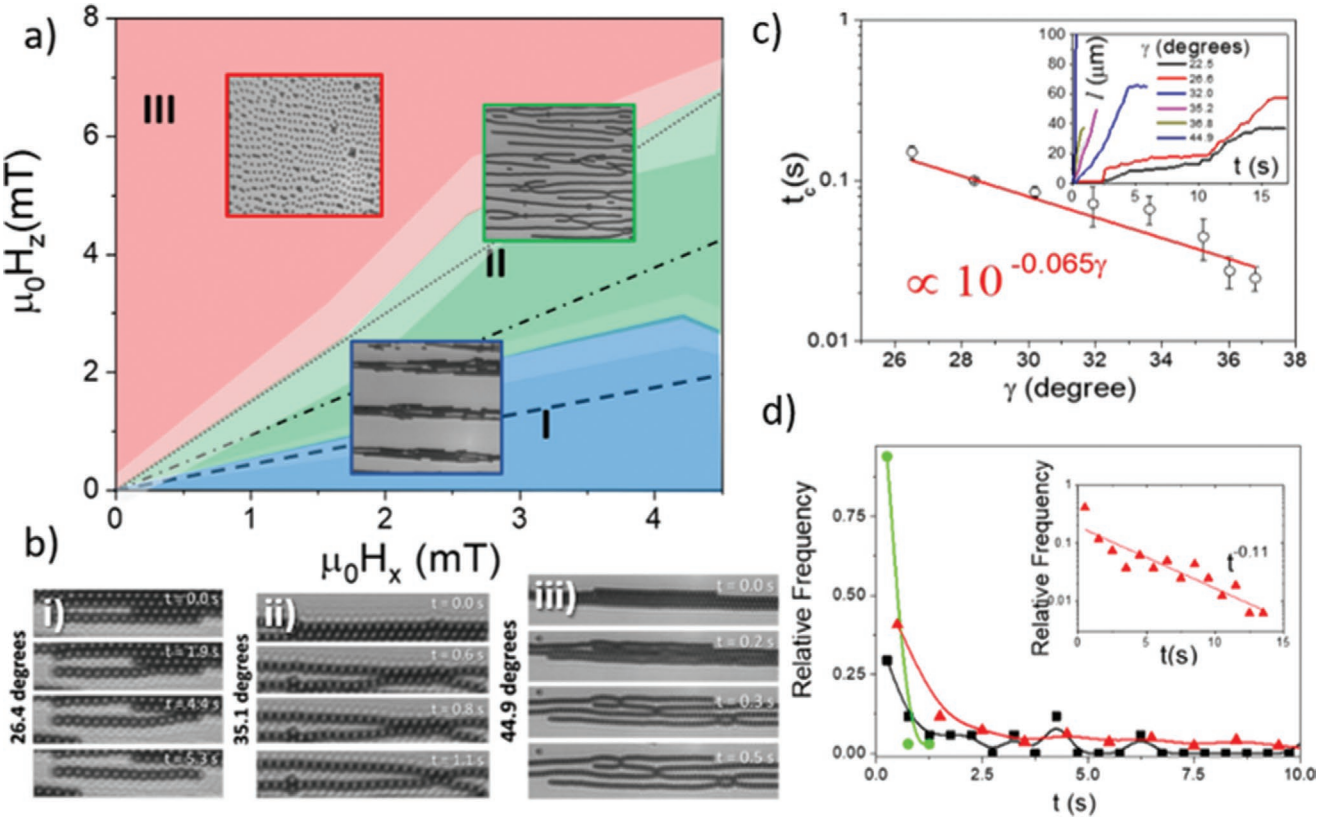

Figure 1. a) State diagram of a monolayer magnetic particles, 2.8 μm in size and adsorbed at an aqueous/decane interface parallel to the *xy* plane, under the action of a tilted field $\vec{H} = \vec{H}_x + \vec{H}_z$. The area fraction is 0.22. In the zone I, the particles aggregate forming chains and bundles oriented along the *x* axis. In the zone II, the fused bundles split into the constituting chains, creating a striped pattern. In the zone III, most of the particles are isolated, and only some of them form small permanent aggregates. The dashed line separates the area where $\gamma = |arctan\ (H_z/H_x)| < \gamma_{c1} \approx 20°$, from the area limited by the dash-dotted lines, where $\gamma_{c1} < \gamma < \gamma_{c2} \approx 37°$. In the area between the dash-dotted and the dotted lines, $\gamma_{c2} < \gamma < \gamma_{c3} \approx 56°$. b) The sequences of video-microscopy images show the gradual/sharp separation of the chains forming different bundles for three values of γ (i, $\gamma = 24.6°$ (Movie S1, Supporting Information), ii, $\gamma = 35.1°$ (Movie S2, Supporting Information), iii, $\gamma = 44.9°$ (Movie S3, Supporting Information)). c) Characteristic time of unzipping, $t_c \equiv a/v$, versus tilt angle of the applied field. In the range from 25° to 37°, this time has an exponential dependence on the tilt angle (red line). In the inset, the time evolution of the distance covered by the propagation, *l*, is represented for different values of γ. d) Relative frequency of the number of unzipping events started a time *t* after applying H_z, for different values of γ (black squares, $\gamma = 22.5°$; red triangles, $\gamma = 28.3°$; green circles, $\gamma = 32.0°$). The inset shows the data measured for the intermediate value, $\gamma = 28.3°$, in a linear-log graph. Here, the red continuous line highlights the exponential dependence of the relative frequency. In Figures b), c) and d), $\mu_0 H_0 = 3.8$ mT.

component H_z leads first to the unzip of the bundles into individual chains, zone II, some of them still connected in hairpin configurations. The absence of such hairpin structures when the system is prepared in other initial conditions both in experiment and in Brownian dynamics simulations[22] leads us to believe that those hairpin configurations are metastable states which eventually should separate into individual chains. For higher values of H_z, the linear structures disintegrate into their constituents, zone III, through different mechanisms (more details in ref. [22]).

In zone II, the aggregated chains maintain their integrity while they occasionally separate along the perpendicular direction. At the beginning of this process, one of the particles, usually located at one of the two ends, jumps over an energy barrier. Subsequently, the induced ejection is gradually propagated along the chains contact area, as the adjacent particles in the chain are forced to follow the expelled colloid.[28] The probability of jumping increases with the tilt angle, defined as $\gamma = |arctan\ (H_z/H_x)|$ (compare the sequence of images in Figure 1b -i,ii and Movies S1 and S2: Supporting Information). Above $\gamma \approx 38°$, the chains initially forming a colloidal ribbon instantaneously separate (Figure 1b-iii and Movie S3: Supporting Information).

In Figure 1c, the characteristic time $t_c \equiv a/v$ is plotted as a function of γ, where v is the longitudinal velocity of the zip-like separation, defined as the distance *l* covered by the longitudinal propagation per unit of time. In the range from 25° to 37°, t_c presents an exponential dependence on the tilt angle $t_c \propto 10^{-0.065\gamma}$. The inset in Figure 1c illustrates the temporal evolution of *l*, which is often interrupted for several seconds at low values of γ (see, for example, the time elapsed between the second and third frames in Figure 1b-i and Movie S1, Supporting Information). For $\gamma > 30°$, the propagation is apparently continuous along the bundle, while for $\gamma > 38°$ the chains separate almost instantaneously. The time taken for the onset of unzipping in different bundles after the perpendicular component H_z is applied is a random event. The distributions of such events for different field tilt angles γ are shown in Figure 1d. For intermediate values,

$\gamma_{c1} \leq \gamma \leq \gamma_{c2}$, a decaying exponential distribution is obtained, log (Relative Frequency)$\propto -0.11t$ for $\gamma = 28.3°$ (see inset in Figure 1d), evidencing that not only the propagation of the unzipping process but also its onset is consistent with an Arrhenius process.

2.1.2. Theoretical Discussion

Throughout this work, gentle magnetic fields are applied, and the paramagnetic particles remain in the linear regime where their magnetic susceptibility is constant. The potential between two induced dipoles $\vec{m}_i, \vec{m}_i$ separated by a distance $\vec{r}_{ij}$ is maximally attractive (repulsive) for particles separated along a direction parallel (perpendicular) to the magnetic field. When the induced dipoles are tilted out of the confining interface, the dipolar interaction between two parallel chains of sizes N_1 and N_2, oriented along the x axis and separated by a distance Δy, can be decomposed in $U^{dd} = U^{dd}_{\parallel} + U^{dd}_{\perp}$, where $U^{dd}_{\parallel} = -\sum_{i=1}^{N_1}\sum_{j=1}^{N_2} \lambda_{\parallel} \frac{2(x_i/a - x_j/a)^2 - (\Delta y/a)^2}{[(\Delta y/a)^2 + (x_i/a - x_j/a)^2]^{5/2}}$ and $U^{dd}_{\perp} = \sum_{i=1}^{N_1}\sum_{j=1}^{N_2} \frac{\lambda_{\perp}}{[(\Delta y/a)^2 + (x_i/a - x_j/a)^2]^{3/2}}$ arise from the interactions between the induced moments parallel, $\vec{m}_{\parallel}$, and perpendicular, $\vec{m}_{\perp}$, to the confining interface, respectively. Here, $\lambda^{ij}_{\parallel,\perp} = \frac{\mu_0 m^i_{\parallel,\perp} m^j_{\parallel,\perp}}{4\pi a^3 k_B T}$, and x_i are the x coordinates of particles. For a constant field of modulus $H_0 = \sqrt{H_z^2 + H_x^2}$, the vertical component of the induced moments and the repulsion between the particles increase with the tilt angle, defined as $\gamma = |arctan(H_z/H_x)|$ (see **Figure 2**a).

In Figure 2b we represent the dipolar magnetic energy per particle of a bundle made of two long chains ($N >> 1$), U^{dd}_{bundle}, and of the two chains infinitely separated, $U^{dd}_{2chains}$, as a function of γ. The energy of the bundle is smaller than that of separate chains for $\gamma \leq \gamma_{c1} \approx 20°$ (area below the dashed line in Figure 1a), but for $\gamma_{c1} \leq \gamma \leq \gamma_{c3} \approx 56°$ the configuration with two separate chains is energetically favorable (area between the dashed and dotted lines in Figure 1a). For $\gamma > \gamma_{c3}$ the monomers repel one another and they become isolated.

In Figure 2c we represent the magnetic energy of interaction per particle, $U^{int} \equiv U^{dd}_{bundle} - U^{dd}_{2chains}$, of two out-of-registry long parallel chains as a function of their lateral distance, for different values of γ. The energy profile evidences that for $\gamma \leq \gamma_{c2} \approx 37°$ there exists an energy barrier that separates the configuration of the two chains in contact from that in which they are far away (area below the dash-dotted line in Figure 1a). The energy barrier is located at a characteristic length named escape distance, which increases with the chain length.[29] The height of the energy barrier per particle, U_B, is represented in the inset of Figure 2c, in units of thermal energy at room temperature. For $\gamma \leq \gamma_{c1}$, the in-contact configuration corresponds to the absolute energy minimum, and the chains remain in the bundled configuration (zone I of Figure 1a). For $\gamma_{c1} \leq \gamma \leq \gamma_{c2}$, the red area in inset of Figure 2c, the bundle configuration is metastable. In this range, which corresponds to the area between the dashed and the dashed-dotted lines in Figure 1a, the thermal energy of the system can promote the transition of the chains over the energy barrier, of decreasing height with increasing γ, to reach the lowest energy state of two chains located apart from one another. The repulsion promoted by the vertical component of the induced dipoles becomes comparable to the energy of the inter-chain bonds, being still much smaller than the bond energy between adjacent particles within the chains. Hence, the aggregated chains maintain their integrity, but they can overcome the energy barrier and separate, beyond the escape distance. This dependence is reminiscent of a thermally activated Arrhenius process,[30] characterized by an attempt frequency and an energy barrier that decreases monotonically with the tilt angle (see inset of Figure 2c), and qualitatively explains the behavior described in Figure 1b–d. Since the end particles are less magnetized by the field generated by the rest of particles, the energy required to break the inter-chain bonds is lower at the ends than in intermediate sites, which explains the preferential disconnection of bonded chains at their ends.[22,31] As soon as the gap between chains is greater than the escape distance (in the range between $2a$ and $3a$ according to Figure 2c) they feel a repulsive interaction and separate.

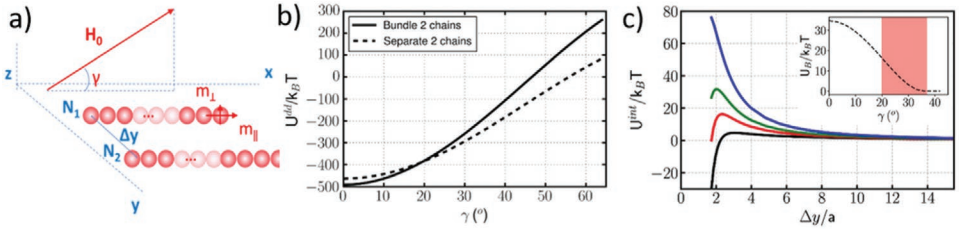

Figure 2. a) The scheme represents two linear aggregates of size N_1 and N_2 adsorbed on the plane xy and separated at a distance Δy upon the influence of a tilted field H_0, with a tilt angle γ. The applied field induces in each particle moments parallel, $\vec{m}_{\parallel}$, and perpendicular, $\vec{m}_{\perp}$, to the confining interface. b) Dipolar magnetic energy per particle of a bundle made of two long chains ($N = 50$) and of the two separated chains as a function of the field tilt angle γ. c) Magnetic dipolar interaction energy per particle between two long parallel chains, in an out-of-registry configuration, as a function of their mutual distance and for different tilt angles: $\gamma = 0°$ (black), $\gamma = 20°$ (red), $\gamma = 30°$ (green), $\gamma = 40°$ (blue). Inset: height of the energy barrier, which separates the configurations with the two chains in contact from the ones where the chains are located far away from one another, as a function of the tilt angle. The red shaded area identifies the region where the configuration in contact is metastable. These calculations are done with the parameters of the superparamagnetic particles employed in experiment ($\chi_v = 0.4$ and radius $a = 1.4$ μm), and the intensity of the field used in related experiments $\mu_0 H_0 = 3.8$ mT (see Figure 1b–d).

2.2. Dynamic Self-Assembly of Floating Pearl Chains

2.2.1. Experimental Results

When the applied field rotates in the plane of the interface $H(t) = H_0(\cos \omega t, \sin \omega t, 0)$, the adsorbed particles tend to assemble in planar hexagonal structures (zone I **Figure 3**a). The application of an extra static magnetic field perpendicular to the interface, H_z, causes a constant tilt of the field with the interface, with a new tilt angle defined as $\gamma = |arctan\ (H_z/H_0)|$, that induces dismantling of the dynamically assembled structures.[6] The perpendicular component induces repulsive dipolar interactions that promote the disintegration of the compact carpets in a cross-linked structure (zone II in Figure 3a) or a set of rotating small aggregates and monomers (zone III in Figure 3a).

The application of an elliptically polarized rotating field of high frequency, $\vec{H}(\omega) = H_{0x}\cos(\omega t)\hat{e}_x + H_{0y}\sin(\omega t)\hat{e}_y$, with a field strength defined as $H_0 \equiv \sqrt{\left(H_{0x}{}^2 + H_{0y}{}^2\right)/2}$, induces either the formation of stable out-of-equilibrium linear chains of particles nearly aligned along the x-axis (which is hereafter identified as the direction of the semi-major axis of the ellipse traced by the field), or the creation of rotating carpets of spinning magnetic particles (zone I, Figure 3b), depending on the value of the elliptic parameter $\beta \equiv (H_{0x}{}^2 - H_{0y}{}^2)/(H_{0x}{}^2 + H_{0y}{}^2)$. The additional application of a constant field perpendicular to the confining plane favors the linear structures, zone II of Figure 3b, or the complete disassembly of the structures, zone III of Figure 3b. The repulsive chains of rotating particles that emerge after applying the vertical component of the field (zone II in Figure 3b) make an angle ϕ^{**} with respect to the x-axis, which depends on the β value (see Figure 3c). Our experiments suggest that the chain orientation is determined by the balance between the magnetic torque and the hydrodynamic drag under time-dependent elliptical actuations in the asynchronous regime.[32] Indeed, very similar orientations are obtained for rigid chains formed with the same magnetic particles, discarding a relevant effect due to the rotation of the colloids. Although there is a torque on the chain caused by the hydrodynamic flows generated by the rotating monomers, its effect should be subdominant for the cases studied here (see the Supporting Information). In Figure 3c, we show the equilibrium angle obtained in experiment as a function of β. For values of $|\beta| < 0.2$, gray zone in Figure 3c, the linear structures disintegrate.

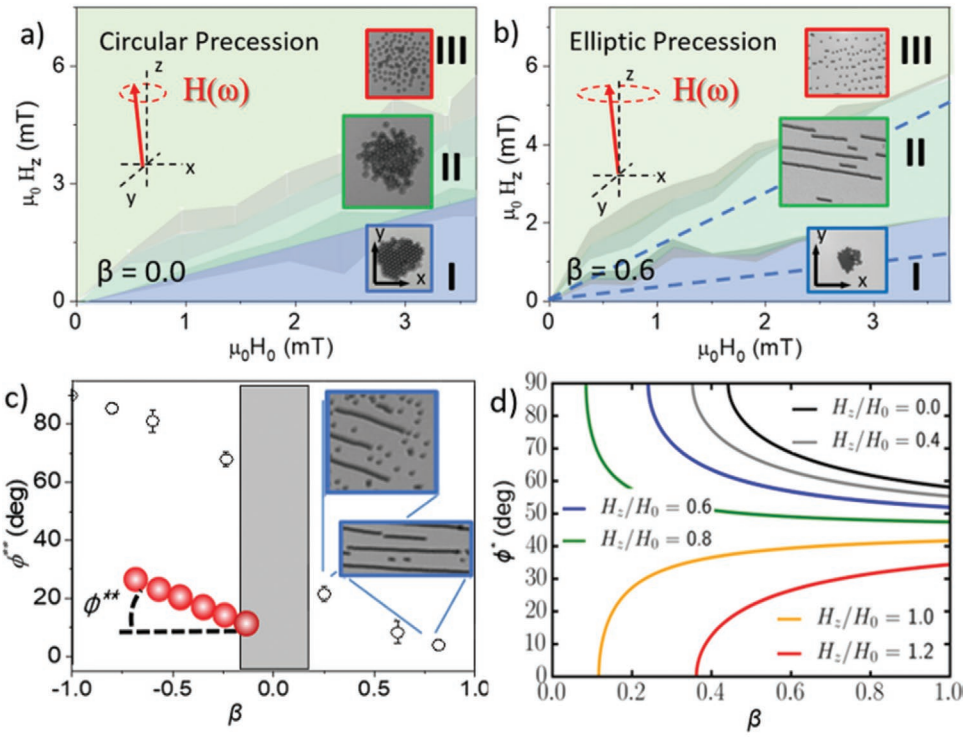

Figure 3. a) State diagram of a rotating planar aggregate made up of magnetic particles after being subjected to a precessing field following a circular trajectory about the axis perpendicular to the confining interface. In the zone I, the particles still form ordered colloidal carpets. In the zone II, the particles form cross-linked structures where the inter-particle bonds continuously break and reform. In the zone III, the planar aggregates disintegrate in the constituent monomers. b) State diagram of a planar aggregate made up of magnetic particles after being subjected to a field following an elliptical trajectory about the axis z perpendicular to the confining interface. In the zones I and III, the response of the planar aggregate is analogous to the one described in a). In the zone II, the rotating cluster transforms in a striped pattern of pearl-chain-like aggregates. The two dashed lines show the theoretically predicted transitions from carpet to chain and from chain to monomers. ($H_z^{(1)}(H_0)$ and $H_z^{(2)}(H_0)$ in the main text). c) The angle ϕ^{**} between the x axis and the chains formed by a precessing field, $\mu_0 H_0 = 1.5$ mT, $\mu_0 H_z = 2.6$ mT as a function of β. In the grey zone, the linear structures disintegrate. In (a–c) $\omega = 125$ rad s^{-1}. d) The dependence of ϕ^* with β is shown for different values of H_z/H_0 (see Equation (2)).

2.2.2. Theoretical Discussion

To understand the formation of such structures under high frequency elliptical fields we consider the time-averaged magnetic pairwise interaction between paramagnetic colloids,[4,33] taking into account local-field corrections due to the presence of the neighboring particles.[5,22] Although many-body interactions can be relevant for concentrated suspensions of magnetic colloids under time-dependent fields,[6,34] only quantitative corrections should be expected in the conditions of our experiments[6] and the qualitative behavior here described should not be altered. When the applied field rotates in the plane of the interface at relatively high frequencies, $f = \omega / 2\pi > 10$ Hz, time averaging of the dipole–dipole interactions gives an effective attractive potential $\langle U^{dd} \rangle = -(\mu_0 m^2/(8\pi(x+\gamma)^3))$, isotropic in the plane of the interface, that leads to the formation of compact and ordered clusters.[4,33] At the same time, the rotating magnetic field promotes the rotation of the composing beads, that in turn induces the rotation of the formed clusters at an angular frequency ω_c, lower than the one imposed by the external field.[35] The torque applied on the rotating particles, always balanced by the viscous torque, appears due to the presence of a small permanent moment within the particles and the finite internal relaxation time of the particle magnetization. In the interfaces studied here, the viscous torque is relatively low, and the spinning particles attain angular velocities of the order of 10 rad s^{-1}.[36]

The time-averaged magnetic potential of two confined and identical paramagnetic particles of radius a separated a distance r when the particles are under the action of a precessing field is given by (see the Supporting Information):

$$U_2^{dd} = -\frac{\mu_0 H_0^2}{8\pi r^3}\left[\chi_\parallel^2\left(1+\beta\cos 2\phi\right) - \chi_\perp^2\left(1-\beta\cos 2\phi + 2(H_z/H_0)^2\right)\right] \quad (1)$$

Here, ϕ is the angle between the particles center-to-center vector and the major axis of the elliptic field, and $\chi_\parallel = \frac{4\pi a^3}{3}\frac{\chi_V}{1-\chi_V/12}$ and $\chi_\perp = \frac{4\pi a^3}{3}\frac{\chi_V}{1+\chi_V/24}$ the magnetic susceptibilities in the particles center-to-center direction and in the perpendicular direction, respectively, when the two particles are in contact. χ_V is the volume susceptibility of the paramagnetic particles. The angular range where two floating particles attract is delimited by:

$$\phi^* = \frac{1}{2}arccos\left[\frac{2\chi_\perp^2(H_z/H_0)^2 - 2\chi_\parallel^2 + \chi_\perp^2}{\beta(2\chi_\parallel^2 + \chi_\perp^2)}\right] \quad (2)$$

which is shown in Figure 3d as a function of β and different values of H_z. For angles $\phi < \phi^*$ the two particles attract, whereas they repel if $\phi > \phi^*$. For $H_z/H_0 < \sqrt{\chi_\parallel^2/\chi_\perp^2 - 1/2}$, the attractive region increases with decreasing $|\beta|$ and decreasing values of H_z. For $H_z/H_0 > \sqrt{\chi_\parallel^2/\chi_\perp^2 - 1/2}$, cases of circular actuations (with $\beta \approx 0$) are unstable and only cases with large values of β have attractive regions. The paramagnetic colloids can form magnetic carpets in a hexagonal lattice if the cone of attraction satisfies $\phi^* > \pi/3$. This condition results in the threshold line $H_z^{(1)} = \left(\sqrt{\frac{2(2-\beta)\chi_\parallel^2 - (2+\beta)\chi_\perp^2}{\chi_\perp^2}}\right)\frac{H_0}{2}$, which indicates the transition from carpet-like (for $H_z < H_z^{(1)}$) to chain-like (for $H_z > H_z^{(1)}$) structures. Note that the carpets only form when $\beta < 2\frac{2\chi_\parallel^2 - \chi_\perp^2}{2\chi_\parallel^2 + \chi_\perp^2}$. The transition from a configuration of chain structures to another of monomers in which magnetic colloids repel one another occurs at $H_z^{(2)} = (\sqrt{\frac{2(1+\beta)\chi_\parallel^2 - (1-\beta)\chi_\perp^2}{2\chi_\perp^2}})H_0$. The predicted transition lines are represented in Figure 3b, in qualitative agreement with experiment. The latter results qualitatively confirm the structure diagram depicted in Figure 3b, which shows that both, the application of H_z and the increased ellipticity of the in-plane component, hinder the conformational change from a linear aggregate to a 2D compact cluster promoted by the application of the rotating field.[37]

2.3. Interfacial Transport of Colloidal Cargos via the Hydrodynamic Flow Field Generated by a Micro-Roller Conveyor

2.3.1. Experimental Results

In the previous section, we illustrated how the application of the elliptic precessing field allows for the ordered dissemination of linear aggregates on the fluid interface. During the process, the chains are quite stable, presenting slow convective displacements. Since the rotating component of the field exerts a torque on the individual particles, forcing them to rotate around an axis perpendicular to the surface, the dynamic structures can be used to generate flows in their proximities. The vortex flows generated by the chain-like aggregates are a manifestation of the external energy injection and can be employed in the active transport of floating non-magnetic colloidal cargos, which become dragged along the chain structures in a similar way to a roller conveyor.[7,33] The transport of the cargo can be easily reverted in the opposite direction by inverting the rotation of the applied field. The generated flow, however, does not force the cargos to remain close to the vicinity of the aggregates, which are free to move away from the chains, in a process favored by the thermal agitation or the presence of convective flows (**Figure 4a** and Movie S4: Supporting Information). The cargos located on one side or another of the chain move in opposite directions (see Figure 4a,b and Movie S5: Supporting Information). Since all chains have the same rotation chirality, the flows generated by adjacent chains cancel out and the transport mechanism is inhibited. As a result, in regions with high density of chains, chiral cargo transport can only take place along the edge or such regions. As the passive particle arrives to the end of the chain, it first orbits around it due to the effect of the flow generated by rotation of the last rotor.[38] Next, the cargo is translated in the opposite direction, the one favored by the rotation of the magnetic particles.

The transport mechanism is analyzed in Figure 4c, where we plot the time evolution of the relative velocity v_{rel} of a cargo of radius $A = 2.8$ μm, together with the time evolution of the distance

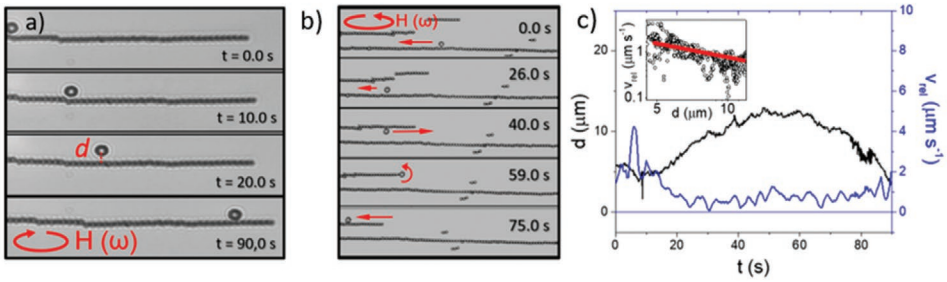

Figure 4. a) (Movie S4, Supporting Information) The sequence of videomicroscopy images shows a non-magnetic polystyrene particle of radius $A = 2.8$ μm travelling along the horizontal thanks to the hydrodynamic flow generated by a pearl-like-chain of rotating particles, subjected to the action of an elliptical precessing field. b) (Movie S5, Supporting Information) The sequence of videomicroscopy images shows how the flow generated by the last colloid, at the chain edges, can redirect the cargo in the opposite direction. c) Time evolution of the distance d between the cargo center and the chain axis together with the relative velocity v_{rel} of a cargo of radius $A = 2.8$ μm, calculated as the horizontal displacement with respect to the transporting chain per unit time. The inset shows the dependence of the relative velocity with the cargo-roller conveyor distance. The red line is a fit to the data in the form given by Equation (5). Here, the unique fitting parameter is $\omega_r = (4.0 \pm 0.1)$ rad s^{-1}. In all these experiments, all the particles are adsorbed on the aqueous/decane interface, and $\mu_0 H_0 = 3.0$ mT, $\beta = 0.83$, $\mu_0 H_z = 2.1$ mT, $\omega = 125$ rad s^{-1}.

d between the cargo center and the chain axis. v_{rel} was calculated as the x displacement with respect to the transporting chain per unit time. The inset of Figure 4c shows that, in contrast to the dragging flow generated by an isolated sphere in the low-Reynolds number limit, that decays asymptotically as d^{-2} from the center of the spinner, the hydrodynamic flow generated by the chain can be phenomenologically seen to decay as $d^{-\xi}$, with $\xi = (1.15 \pm 0.06)$.

2.3.2. Theoretical Discussion

To explain this experimental result, we must consider that the cargo is advected by the flow generated by the whole chain. The hydrodynamic flow generated on an adsorbed passive colloid by a long magnetic chain, directed along the x axis, whose component particles rotate with $\vec{\omega}_r = \omega_r \hat{e}_z$, is approximately given by $\vec{u} = (u_x, 0, 0)$ with (see the Supporting Information):

$$u_x = a^2 \omega_r \left(\frac{d}{d^2 + (A-a)^2} + \frac{1-\psi}{1+\psi} \frac{d}{\left(d^2 + (A+a)^2\right)} \right) \tag{3}$$

where $\Psi = \eta_1/\eta_2$, and η_1, η_2 are the viscosities of the decane and aqueous fluid phases, respectively. The direction of the flow is given by the sense of rotation. Note that the angular velocity ω_r is determined by the balance between the magnetic and viscous torques on the rotating colloids, and thus the speed of the cargo u_x decrease for increasing solvent viscosities. Equation (3) justifies the exponent $1 < \xi < 2$ obtained in the phenomenological exponential fit of the flow dependence with d. In the inset of Figure 4c, the experimental data are properly fitted by Equation (3), with $\omega_r = (4.0 \pm 0.1)$ rad s^{-1} as the only fitting parameter. At the chain edges, the flow is dominated by the rotation of the last particle, and

$$\vec{u} \approx a^3 (a+A) \omega_r \left(\frac{1}{(a+A)^2 + (a-A)^2} + \frac{1-\psi}{1+\psi} \frac{1}{2^{3/2}(a+A)^3} \right) \hat{e}_\theta \tag{4}$$

where we have assumed that the passive colloid is in contact with the chain, $\hat{e}_\theta = (-\sin\theta, \cos\theta, 0)$ is the azimuthal unit vector and θ the angle between the cargo position vector from the last colloid in the chain $\vec{r}$ and the x axis. Equation (4) qualitatively confirms the motion described by the passive particle in Figure 4b when it reaches the end of the chain.

3. Conclusion

The application of time-dependent magnetic fields has been shown to induce the formation of a large collection of dynamic self-assembled structures of magnetic colloids, encompassing unstable fronts, flocks and ribbons of ferromagnetic micro-rollers,[39] microtubes of magnetic Janus particles[40] or worms, walkers, carpets and sheets of superparamagnetic colloids.[4,7,33,41] Such complex assemblies are supported by a continuous injection of energy into the system,[42] and can be used as models to study a wide range of non-equilibrium phenomena, such as out of equilibrium organization (applicable to biological structures) or the transport of matter in the low Reynolds number regime.[43]

In this work, we have shown, both theoretically and in experiment, that the confinement at a fluid–fluid interface of paramagnetic colloids under external magnetic fields permits the emergence of new static and dynamical stationary structures which have not been observed in bulk dispersions. The modulation of the applied field leads to the transition between cross-linked aggregates and carpets, to new assemblies composed by static and dynamic pearl-chain-like structures that can be used in new strategies of micro-manipulation. The latter are only feasible upon strong 2D confinement conditions, here optimally reached by using particles adsorbed at a water-decane fluid interface.

We have characterized the transition from bundles of chains to pearl-like-chain assemblies and isolated monomers, as a static component of the magnetic field perpendicular to the interface is added to a static field applied on the plane of the interface. We have found that such transition occurs due to a different dependence of the dipolar energies of bundles and chains on the field tilt angle, with a stronger monotonic increase in the former than in the latter, and we have determined the threshold angle γ_{c1} that governs the transition from bundle to separate

chains, with good agreement with our experiments. We have also shown how the dynamics of the transition depends on the field tilt angle. The evolution of the transition from bundles to chains occurs as a random activated process for lower tilt angles, while it is a deterministic almost instantaneous event for higher values of γ. For low angles, $\gamma_{c1} < \gamma < \gamma_{c2}$, the bundled structure is a metastable state and the transition occurs as an unzipping mechanism that starts at an edge and propagates along the bundle, with a velocity which increases exponentially with the tilt angle, reminiscent of a thermally activated Arrhenius event. For high angles, $\gamma > \gamma_{c2}$, the transition occurs instantaneously and simultaneously along the bundle.

Then, we have investigated the steady self-assembled structures of magnetic colloids that arise under circularly and elliptically polarized time-dependent rotating fields, on the plane of the interface, when we add a static component of the magnetic field perpendicular to the interface. We have detected a transition from rotating carpets of rotating magnetic particles to stationary pearl-chain-like assemblies of rotating monomers or to rotating isolated monomers, as a function of the tilt angle of the field with the interface and the degree of ellipticity of the time-dependent actuation. The results, rationalized with the help of a mutual time-averaged dipolar interaction between the paramagnetic colloids under the time-dependent field, which includes local field effects, explain the transitions observed in other non-confined systems, when colloids float on a solid substrate.[4–7,24,25] We have derived analytic expressions for the transition lines in terms of the parameters of the field (ellipticity and magnitudes) and the particles (volume susceptibility), that are in good agreement with experiment and can help to explain the transitions observed in other non-confined systems.[7,37,41]

Finally, we have devised a new way for the steering of non-magnetic micron-sized particles along the parallel pearl-like-chains of rotating magnetic colloids, all of them adsorbed onto the fluid interface. Unlike previous strategies developed for transporting objects trapped at fluid interfaces, which use interfacial physical effects such as Marangoni effects,[44] gradients in concentration,[45] the self-generation of standing waves,[16c] magnetocapillary effects[46] or the modulation of the potential generated by asymmetrically adsorbed magnetic particles,[17] in this work the passive particles are dragged by the hydrodynamic conveyor belt generated by the rolling species, through a strategy that can be monitored via the application of suitable magnetic manipulation techniques and does not need of direct contact with the cargo. The chain structures created by such actuations demarcate lanes along which adsorbed cargos can be transported. The generated flows lack a component that attracts cargos to the linear aggregate, and the transport efficiency needs of a supplementary mechanism that helps to keep the cargos close to the activated micro-device, allowing for uninterrupted transport. In this regard, strategies based on the use of capillary interactions are good candidates, but they will require of particles with larger wetting angles, and/or larger or anisotropic particles, capable of induce long-ranged attractive interactions.[47] In addition to the use of these patterns of rotating colloids as a transport mechanism in fluid interfaces and microfluidic devices, they can be employed to mix adsorbed molecules or accelerate surface-chemical reactions, overcoming diffusion limitations. Besides, the capability of these dynamic structures to create hydrodynamic fluxes of opposite direction in different regions of the interface suggests that they could be employed to design 2D acoustic metamaterials.[48,49] These systems use regular arrangements of fluid flows to hamper sound propagation for certain frequency bands in the interior of the material while it is permitted at its edges.[49] The resulting structures can be transferred as mono- or multilayers onto solid supports for the production of materials with novel magnetic, optical, thermal and/or mechanical properties.[50] While experiments were performed with particles of 1.4 μm radius a, the conclusions should hold for smaller particles (with radius in the hundreds of nanometers) for which both the magnetic and capillary interactions exceed thermal effects.

4. Experimental Section

The superparamagnetic particles employed in this work are spherical microparticles, composed by a polystyrene matrix evenly doped with superparamagnetic iron oxide nano-grains and stabilized in water by surface carboxylic groups, with average sizes of a = 1.4 μm, density ρ = 1.3 gcm^{-3} and magnetic susceptibility under static field χ_v = 0.4 (Dynabeads M-270, Invitrogen). The passive cargos consist of surfactant-free polystyrene microparticles with radius A = 2.85 μm, negatively charged with sulfate functional groups and charge density 6.2 μC cm^{-2} (Interfacial Dynamics, USA). All the colloidal solutions were washed twice in Milli-Q water to remove the surfactant that may have been employed during the synthesis. After sonication for 5 min, small volumes (10–100 μL) are injected with a Pasteur pipette into the subphase, close to a flat interface at 25 °C. The upper liquid phase was decane, with density ρ = 950 kg m^{-3} and viscosity $\eta_1 = 8.5 \times 10^{-4}$ Pa s^{-1} (Dow Corning Corporation), whereas the lower liquid phase was a solution of Dodecyltrimethylammonium bromide (DTAB) 5×10^{-6} M in water, with density ρ = 108 kg dm^{-3} and viscosity $\eta_2 = 8.9 \times 10^{-4}$ Pa s. Since the heavy magnetic particles tend to sediment due to their relatively high size and density, they are led to the upper interface thanks to the field gradient created by approaching a neodymium magnet for several seconds. The cationic surfactant present in the aqueous phase screens the electrostatic repulsion between the negatively charged particles and the decane/aqueous interfase, allowing the colloids to breach the charged surface.[51] Since the surface energy of the system enormously decreases after the adsorption of the particles,[52] these become robustly arrested at the fluid interface.[53] The adsorbed particles are mostly immersed in the aqueous phase (see the SEM images of the magnetic particles obtained with the Gel Trapping Technique (GET) in ref. [22]), do not display order due to long-ranged dipole–dipole electrostatic repulsions,[25] neither aggregate due to capillary interactions, even at high surface coverages.[26]

The loaded interface is energized by a time-dependent external field, generated by of a pair of coils connected in series, aligned along the x and y axis, while a fifth coil is aligned along the optical axis, in the plane of the studied system. The x-y coils are connected to a power amplifier (Kepco BOP 2 × 20-10D) commanded by a waveform generator (National Instruments 9269), and the z coil is connected to a DC power supply (Tenma, 72–2805), and the resultant constant field is constant when applied along the xz plane, or precesses around the z axis at an angular frequency ω. The actuated monolayer is monitored with an upright optical microscope (BH2, Olympus) connected to a CCD camera (EO1312M, Edmund) equipped with a 40 × 0.65 NA and a 20 × 0.40 NA objective.

Supporting Information

Supporting Information is available from the Wiley Online Library or from the author.

Acknowledgements

This work was partially funded by Horizon 2020 program through 766972-FET-OPEN21 NANOPHLOW and Ministerio de Ciencia e Innovación (Grants No. PID2019-105343GB-I00 and PID2019-106557GB-C21). F.M.-P. acknowledges support from MINECO (Grant No. RYC-2015-18495) and UCM/SANTANDER 2019 (PR87/19)-22536.

Conflict of Interest

The authors declare no conflict of interest.

Data Availability Statement

The data that support the findings of this study are available from the corresponding author upon reasonable request.

Keywords

2D confined systems, colloidal transport, dynamic self-assembly, fluid interface, superparamagnetic particles

Received: February 26, 2021
Revised: March 31, 2021
Published online: May 21, 2021

[1] J. S. Andreu, J. Camacho, J. Faraudo, *Soft Matter* **2011**, *7*, 2336.
[2] J. Faraudo, J. S. Andreu, C. Calero, J. Camacho, *Adv. Funct. Mater.* **2016**, *26*, 3837.
[3] a) F. Pietra, F. T. Rabouw, P. G. van Rhee, J. van Rijssel, A. V. Petukhov, B. H. Erné, P. C. M. Christianen, C. de Mello Donegá, D. Vanmaekelbergh, *ACS Nano* **2014**, *8*, 10486; b) H. Massana-Cid, F. Meng, D. Matsunaga, R. Golestanian, P. Tierno, *Nat. Commun.* **2019**, *10*, 2444; c) A. Spatafora-Salazar, D. M. Lobmeyer, L. H. P. Cunha, K. Joshi, S. L. Biswal, *Soft Matter* **2021**, *17*, 1120.
[4] N. Osterman, I. Poberaj, J. Dobnikar, D. Frenkel, P. Ziherl, D. Babić, *Phys. Rev. Lett.* **2009**, *103*, 228301.
[5] J. E. Martin, A. Snezhko, *Rep. Prog. Phys.* **2013**, *76*, 126601.
[6] K. Müller, N. Osterman, D. Babič, C. N. Likos, J. Dobnikar, A. Nikoubashman, *Langmuir* **2014**, *30*, 5088.
[7] F. Martinez-Pedrero, A. Ortiz-Ambriz, I. Pagonabarraga, P. Tierno, *Phys. Rev. Lett.* **2015**, *115*, 138301.
[8] a) M. Wang, L. He, Y. Yin, *Mater. Today* **2013**, *16*, 110; b) A. Tokarev, Y. Gu, A. Zakharchenko, O. Trotsenko, I. Luzinov, K. G. Kornev, S. Minko, *Adv. Funct. Mater.* **2014**, *24*, 4738; c) O. Trotsenko, A. Tokarev, A. Gruzd, T. Enright, S. Minko, *Nanoscale* **2015**, *7*, 7155.
[9] a) C. T. Yavuz, A. Prakash, J. T. Mayo, V. L. Colvin, *Chem. Eng. Sci.* **2009**, *64*, 2510; b) J. Lim, S. P. Yeap, S. C. Low, *Sep. Purif. Technol.* **2014**, *123*, 171.
[10] D. X. Chen, G. Via, F. J. Xu, C. Navau, A. Sanchez, H. C. Gu, J. S. Andreu, C. Calero, J. Camacho, J. Faraudo, *J. Appl. Phys.* **2011**, *110*, 073917.
[11] Z. Lin, X. Fan, M. Sun, C. Gao, Q. He, H. Xie, *ACS Nano* **2018**, *12*, 2539.
[12] B. P. Binks, *Langmuir* **2017**, *33*, 6947.
[13] a) R. Zangi, *J. Phys.: Condens. Matter* **2004**, *16*, S5371; b) G. Algara-Siller, O. Lehtinen, F. C. Wang, R. R. Nair, U. Kaiser, H. A. Wu, A. K. Geim, I. V. Grigorieva, *Nature* **2015**, *519*, 443.
[14] P. Digregorio, D. Levis, A. Suma, L. F. Cugliandolo, G. Gonnella, I. Pagonabarraga, *Phys. Rev. Lett.* **2018**, *121*, 098003
[15] K. Zahn, R. Lenke, G. Maret, *Phys. Rev. Lett.* **1999**, *82*, 2721.
[16] a) A. Snezhko, I. Aranson, W.-K. Kwok, *Phys. Rev. E* **2006**, *73*, 041306; b) F. Martinez-Pedrero, A. Cebers, P. Tierno, *Soft Matter* **2016**, *12*, 3688; c) A. Snezhko, I. S. Aranson, *Nat. Mater.* **2011**, *10*, 698.
[17] F. Martínez-Pedrero, F. Ortega, R. G. Rubio, C. Calero, *Adv. Funct. Mater.* **2020**, *30*, 2002206.
[18] B. A. Grzybowski, H. A. Stone, G. M. Whitesides, *Nature* **2000**, *405*, 1033.
[19] W. Wang, J. Giltinan, S. Zakharchenko, M. Sitti, *Sci. Adv.* **2017**, *3*, 1602522.
[20] a) G. Kokot, D. Piet, G. M. Whitesides, I. S. Aranson, A. Snezhko, *Sci. Rep.* **2015**, *5*, 9528; b) K. Han, G. Kokot, S. Das, R. G. Winkler, G. Gompper, A. Snezhko, *Sci. Adv.* **2020**, *6*, eaaz8535.
[21] a) S. Cappelli, Q. Xie, J. Harting, A. M. de Jong, M. W. J. Prins, *New Biotechnol.* **2015**, *32*, 420; b) G. B. Davies, T. Krüger, P. V. Coveney, J. Harting, F. Bresme, *Soft Matter* **2014**, *10*, 6742.
[22] F. Martínez-Pedrero, F. Ortega, J. Codina, C. Calero, R. G. Rubio, *J. Colloid Interface Sci.* **2020**, *560*, 388.
[23] W. Wen, L. Zhang, P. Sheng, *Phys. Rev. Lett.* **2000**, *85*, 5464.
[24] G. Boniello, Ch. Blanc, D. Fedorenko, M. Medfai, N. B. Mbarek, M. In, M. Gross, A. Stocco, M. Nobili, *Nat. Mater.* **2015**, *14*, 908.
[25] a) P. Pieranski, *Phys. Rev. Lett.* **1980**, *45*, 569; b) R. Aveyard, B. P. Binks, J. H. Clint, P. D. I. Fletcher, T. S. Horozov, B. Neumann, V. N. Paunov, J. Annesley, S. W. Botchway, D. Nees, A. W. Parker, A. D. Ward, A. N. Burgess, *Phys. Rev. Lett.* **2002**, *88*, 246102.
[26] a) B. J. Park, E. M. Furst, *Soft Matter* **2011**, *7*, 7676; b) S. Cappelli, A. M. de Jong, J. Baudry, M. W. J. Prins, *Langmuir* **2017**, *33*, 696.
[27] F. Martínez-Pedrero, M. Tirado-Miranda, A. Schmitt, J. Callejas-Fernández, *Phys. Rev. E* **2007**, *76*, 011405.
[28] F. Martinez-Pedrero, P. Tierno, T. H. Johansen, A. V. Straube, *Sci. Rep.* **2016**, *6*, 19932.
[29] M. Mohebi, N. Jamasbi, J. Liu, *Phys. Rev. E* **1996**, *54*, 5407.
[30] J. Guery, E. Bertrand, C. Rouzeau, P. Levitz, D. A. Weitz, J. Bibette, *Phys. Rev. Lett.* **2006**, *96*, 198301.
[31] S. Melle, O. G. Calderón, M. A. Rubio, G. G. Fuller, *Phys. Rev. E* **2003**, *68*, 041503.
[32] G. Helgesen, P. Pieranski, A. T. Skjeltorp, *Phys. Rev. Lett.* **1990**, *64*, 1425.
[33] J. Yan, S. C. Bae, S. Granick, *Adv. Mater.* **2015**, *27*, 874.
[34] I. M. Kulić, M. L. Kulić, *Phys. Rev. Lett.* **2013**, *111*, 198301.
[35] F. Martinez-Pedrero, P. Tierno, *Phys. Rev. Appl.* **2015**, *3*, 051003.
[36] X. J. A. Janssen, A. J. Schellekens, K. van Ommering, L. J. van Ijzendoorn, M. W. J. Prins, *Biosens. Bioelectron.* **2009**, *24*, 1937.
[37] N. Casic, S. Schreiber, P. Tierno, W. Zimmermann, T. M. Fischer, *EPL* **2010**, *90*, 58001.
[38] Z. Ouyang, J.-Z. Lin, X. Ku, *Phys. Fluids* **2017**, *29*, 103301.
[39] a) M. Driscoll, B. Delmotte, M. Youssef, S. Sacanna, A. Donev, P. Chaikin, *Nat. Phys.* **2017**, *13*, 375; b) F. Martinez-Pedrero, E. Navarro-Argemí, A. Ortiz-Ambriz, I. Pagonabarraga, P. Tierno, *Sci. Adv.* **2018**, *4*, eaap9379; c) A. Kaiser, A. Snezhko, I. S. Aranson, *Sci. Adv.* **2017**, *3*, 1601469.
[40] J. Yan, M. Bloom, S. C. Bae, E. Luijten, S. Granick, *Nature* **2012**, *491*, 578.
[41] C. E. Sing, L. Schmid, M. F. Schneider, T. Franke, A. Alexander-Katz, *Proc. Natl. Acad. Sci. USA* **2010**, *107*, 535.
[42] F. Li, D. P. Josephson, A. Stein, *Angew. Chem., Int. Ed.* **2011**, *50*, 360.
[43] a) E. Karsenti, *Nat. Rev. Mol. Cell Biol.* **2008**, *9*, 255; b) B. A. Grzybowski, C. J. Campbell, *Chem. Eng. Sci.* **2004**, *59*, 1667.
[44] E. Bormashenko, Y. Bormashenko, R. Grynyov, H. Aharoni, G. Whyman, B. P. Binks, *J. Phys. Chem. C* **2015**, *119*, 9910.
[45] a) X. Wang, M. In, C. Blanc, A. Würger, M. Nobili, A. Stocco, *Langmuir* **2017**, *33*, 13766; b) K. Dietrich, G. Volpe,

M. N. Sulaiman, D. Renggli, I. Buttinoni, L. Isa, *Phys. Rev. Lett.* **2018**, *120*, 268004.
[46] G. Grosjean, M. Hubert, G. Lagubeau, N. Vandewalle, *Phys. Rev. E* **2016**, *94*, 021101.
[47] V. M. Starov, M. G. Velarde, *Wetting and Spreading Dynamics*, 2nd ed., CRC Press, Boca Raton, FL **2019**.
[48] R. Fleury, D. L. Sounas, C. F. Sieck, M. R. Haberman, A. Alù, *Science* **2014**, *343*, 516.
[49] S. A. Cummer, J. Christensen, A. Alù, *Nat. Rev. Mater.* **2016**, *1*, 16001.
[50] a) T. Honold, K. Volk, A. Rauh, J. P. S. Fitzgerald, M. Karg, *J. Mater. Chem. C* **2015**, *3*, 11449; b) R. van Dommelen, P. Fanzio, L. Sasso, *Adv. Colloid Interface Sci.* **2018**, *251*, 97.
[51] E. C. Mbamala, H. H. v. Grünberg, *J. Phys.: Condens. Matter* **2002**, *14*, 4881.
[52] B. P. Binks, S. O. Lumsdon, *Langmuir* **2000**, *16*, 8622.
[53] a) V. Poulichet, V. Garbin, *Proc. Natl. Acad. Sci. USA* **2015**, *112*, 5932; b) D. M. Kaz, R. McGorty, M. Mani, M. P. Brenner, V. N. Manoharan, *Nat. Mater.* **2011**, *11*, 138.